Journal of Applied Polymer Science

Microconfinement effect on gas barrier and mechanical properties of multilayer rigid/soft thermoplastic polyurethane films

Rongzhi Huang,[1] Priyakrit Chari,[1] Jung-Kai Tseng,[1] Guojun Zhang,[1] Mark Cox,[2] Joao M. Maia[1]

[1]Department of Macromolecular Science and Engineering, CLiPS – NSF Center for Layered Polymeric Systems, Case Western Reserve University, Cleveland, Ohio

[2]Lubrizol Advanced Materials, Inc., Cleveland, Ohio

Correspondence to: J. M. Maia (E-mail: joao.maia@case.edu)

ABSTRACT: In this article, rigid/soft thermoplastic polyurethane (TPU) films were produced *via* layer-multiplying co-extrusion and the effect of confinement on morphology and gas barrier and mechanical properties is studied. The soft TPU, which is 52% hard-segment, shows phase separation, while the rigid, 100% hard-segment TPU exhibits amorphous structures. Even though the viscosity ratio of the two TPUs is over 10 and the elasticity ratio around 100, optical and atomic force microscopies show that a multilayer structure was successfully achieved. Then, the multilayer TPU films were uni-axially stretched to different amounts of deformations, from 0% to 300%. DSC and WAXS results show that microconfinement occurs during orientation, which causes a significant reduction in oxygen permeability of multilayer TPU films, when stretched at 75%, by comparison to the mono and bi-layer TPU. The dependence of gas barrier properties on temperature and deformation was also investigated, and a 100% improvement in elongation at break was found when compared to films of the rigid TPU. © 2015 Wiley Periodicals, Inc. J. Appl. Polym. Sci. **2015**, *132*, 41849.

KEYWORDS: films; polyurethanes; rheology

Received 17 July 2014; accepted 2 October 2014

DOI: 10.1002/app.41849

INTRODUCTION

Thermoplastic polyurethane (TPU) is an important elastomer exhibiting high melt strength, good mechanical properties, and excellent abrasion resistance, with many intricate applications ranging from biomaterials to footwear.[1–4] By tuning the composition of hard-segments and soft-segments during TPU synthesis, the material created can show a wide range of properties. It is well known that the gas barrier and mechanical properties of TPU depend on the amounts of hard-segments, which have a higher glass transition temperature than soft-segments.[5–7] The issue with the particular material is that with more hard-segments, the material becomes more rigid, and as a result, is not flexible enough for a number of applications, e.g., packaging. Soft-segments play an important role in phase separation *via* different chain lengths, chain extender structures and molecular weight of soft segments.[8,9] When analyzing the balance of mixing relative fractions of hard and soft phases and its effect on the glass transition temperature, studies have shown that hydrogen bonding with ester groups is stronger than with ether groups.[10] Thus, by integrating ester groups, a stronger and more flexible material can be produced. Finding a good balance between these two phases will yield a material that has hard and soft phases, but also flexibility needed for various applications.[7–10] For example, if a TPU can be designed to contain both good gas barrier and flexibility characteristics, then devices such as biomedical bags/tubes can be produced.

Creating multilayered polymeric systems through co-extrusion and biaxial stretching yields favorable characteristics, such as ultra-low gas permeability, high dielectric performance, gradient refractive index lens, 1-D photo crystals, and 3-D storage.[11–20] The purpose of using this layer-multiplying co-extrusion is to control the layer compositions and thickness of two polymers, and in doing so, allowing the maximization of the effect of hierarchical structures and nanoconfinement of the polymers.[21–25] Such an effect can also be achieved by adding nanofillers into polymer matrix forming nanocomposites. For example, Dekun *et al.* have shown that adding organically modified nanoclays into TPU can decrease the gas permeability of the nanocomposites.[26] However, several issues have to be pointed out: first, such an improvement on barrier properties requires a very high amount of nanoclays, e.g. 10 wt %, which, on the other hand, decreases the elongation at break and tensile strength of TPU. Second, homogeneous distribution and exfoliated dispersion of nanoclays in TPU system is very difficult to achieve, especially at high contents of nanoclays where lots of agglomerations appear. The nano-confinement of polymer chains because of

multilayered co-extrusion is able to not only improve the strength of the material, but also significantly enhance the gas barrier properties especially when the individual layer thickness is around 30 nm, and single crystalline orientation is created.[27–29] This indicates that with a multilayer structure, the orientation of the crystalline structure is altered and can be manipulated to improve the mechanical properties and barrier properties of the TPU while maintaining the flexibility.

Even though the structural changes at the microscale upon uniaxial stretching of TPU with various ratios of hard-segments are extensively studied, the uniaxial stretching on multilayer TPU under microconfinement has never been studied.[30,31] In this article, a flexible soft TPU, TPU A, and an engineering TPU commercially available from Lubrizol Advanced Materials, TPU B, are multilayered by continuous layer multiplication co-extrusion. TPU A works well in applications where the polymer is required to be flexible, but it does not have strong gas barrier properties because of its rubbery nature of the soft segments. By contrast, TPU B consists of 100% hard-segments and has excellent gas barrier properties, but it is too rigid for various applications. When these two materials are multilayered, the resulting material is aimed to possess both high gas barrier properties, and relatively good flexibility.

EXPERIMENTAL

Two aromatic, polyester-based TPUs provided by Lubrizol Advanced Materials, were used in this study. Although the exact compositions are proprietary, one of the materails is a rigid TPU, TPU B, consisting of 100% hard-segments, while the second is a soft polyester based TPU, TPU A, with 52% hard-segment. Both materials were dried at 80°C for 24 hours prior to processing. About 1.5 wt % external lubricants (TR 251) provided by Struktol Company, which mainly compose unsaturated primary amide, were added into TPU during co-extrusion.[32,33] Extensional rheometry experiments were performed in a SER device coupled to a Paar Physica MCR 501 rheometer at 175°C. Sample preparation and loading followed the procedure recommended by Barroso *et al.*,[34] in order to ensure the samples were stress-free and not sagging at the beginning of the experiments.

The co-extrusion processing conditions were determined based on the shear rheological properties of TPU B and TPU A characterized by rotational rheometry (Thermo Fisher MARS III) at 205°C. Since these two TPUs are rheologically mismatched, 205°C was chosen as the co-extrusion temperature at which viscoelasticity ratio (the viscosity and elasticity ratio of two polymers at a certain shear rate and temperature) is minimum within the processing window. The combination of a 9-layer

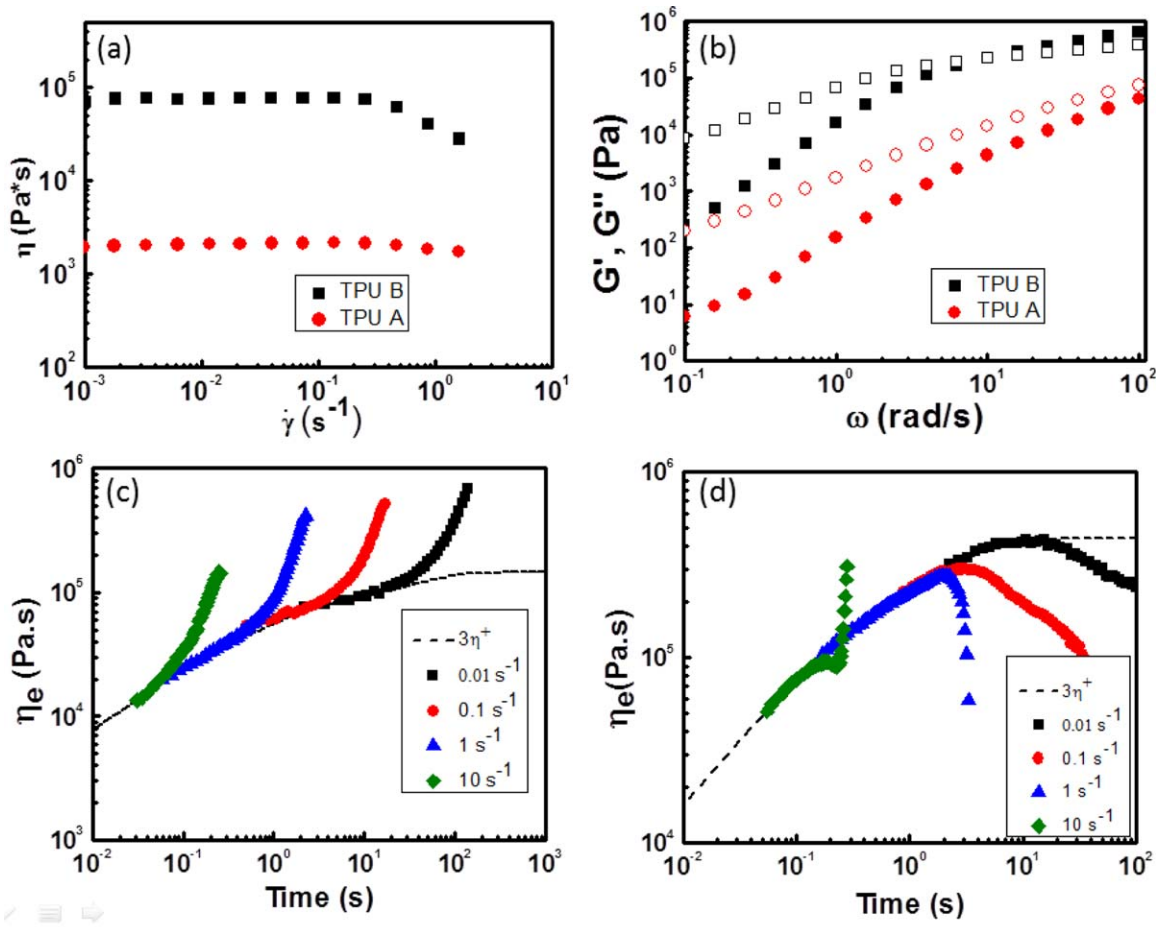

Figure 1. Rheological results of TPUs: (a) steady shear mode and (b) oscillation shear mode; (c) extensional rheology for TPU A, and (d) TPU B. [Color figure can be viewed in the online issue, which is available at wileyonlinelibrary.com.]

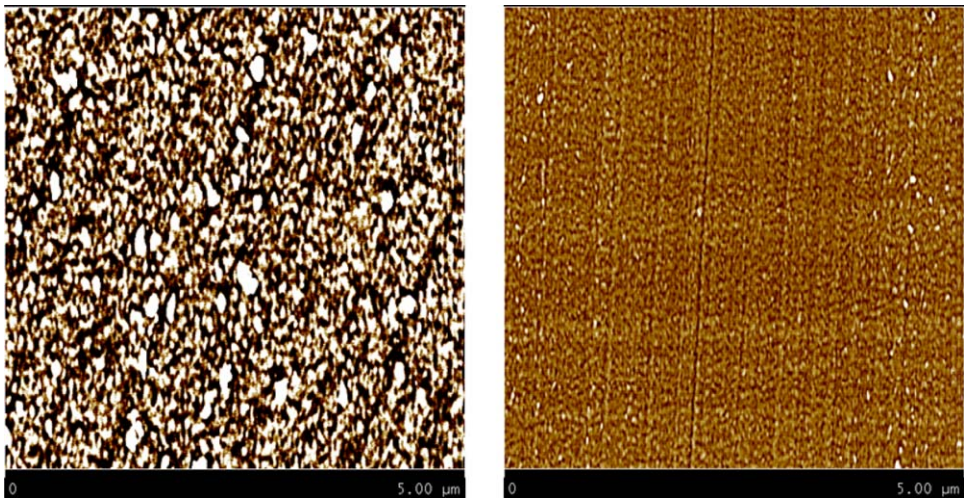

Figure 2. AFM phase images of TPU A (left), and TPU B (right). [Color figure can be viewed in the online issue, which is available at wileyonlinelibrary.com.]

feedblock and a second generation multiplier dies recently developed by the authors is used to produce 65-layer TPU films.[32,33,35] The flow rates of the TPU melts were the same and set by identical gear pumps. Films were extruded through a 7.62 cm coat-hanger die and collected on a stainless take-off roller with temperature set at 80°C. Mono-layer and bi-layer TPU B and TPU A films of 175 μm were also produced.

Film samples with dimension of 7.6 cm × 5 cm × 0.035 cm were prepared for uniaxial stretching. A MTS Alliance RT/30 testing machine at a gage length of 3 cm was used to stretch the samples along the extrusion direction at 100°C, 110°C, 120°C, and 130°C. At these temperatures, the films were stretched to strain of 25%, 50%, 75%, 100%, 200%, and 300% with a deformation rate of 50% per min. After stretching, the samples were held tightly and slowly cooled down to room temperature (the estimated cooling rate is 10°C/min).

The mechanical tests of TPU films, stress–strain curves, were performed with a MTS Alliance RT/30 testing machine. TPU films were cut into "dog-bone" shapes with dimension of 0.44 cm × 0.035 cm and uniaxially stretched until break at room temperature with deformation rate of 50% per min.

Differential scanning calorimetric (DSC, TA Instruments Q-100) measurements were performed on both as-extruded and stretched TPU films ranging from −50°C to 250°C at a heating/cooling rate of 10°C per min with sample sizes of 5–8 mg.

Two dimensional wide angle X-ray scattering (WAXS) measurements were carried out on mono-, bi-, nominal 65-layer films with different percentage of stretching in the normal direction (ND) to characterize the molecular structure and orientation of the TPUs. WAXS experiments were performed under vacuum and at room temperature (25°C), with an X-ray beam based on

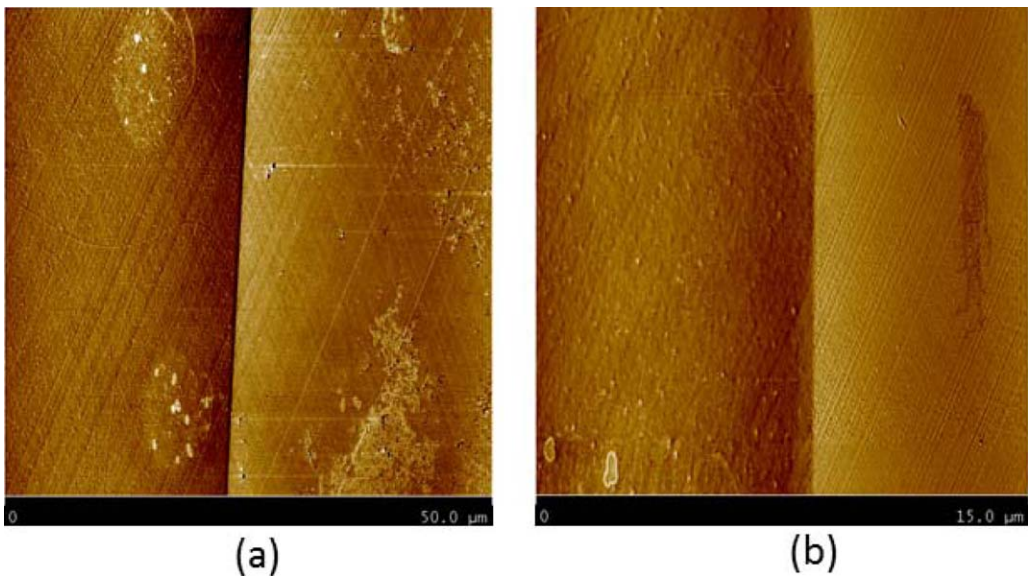

Figure 3. AFM phase images of bilayer TPU B/TPU A: low magnification (left), high magnification (right). [Color figure can be viewed in the online issue, which is available at wileyonlinelibrary.com.]

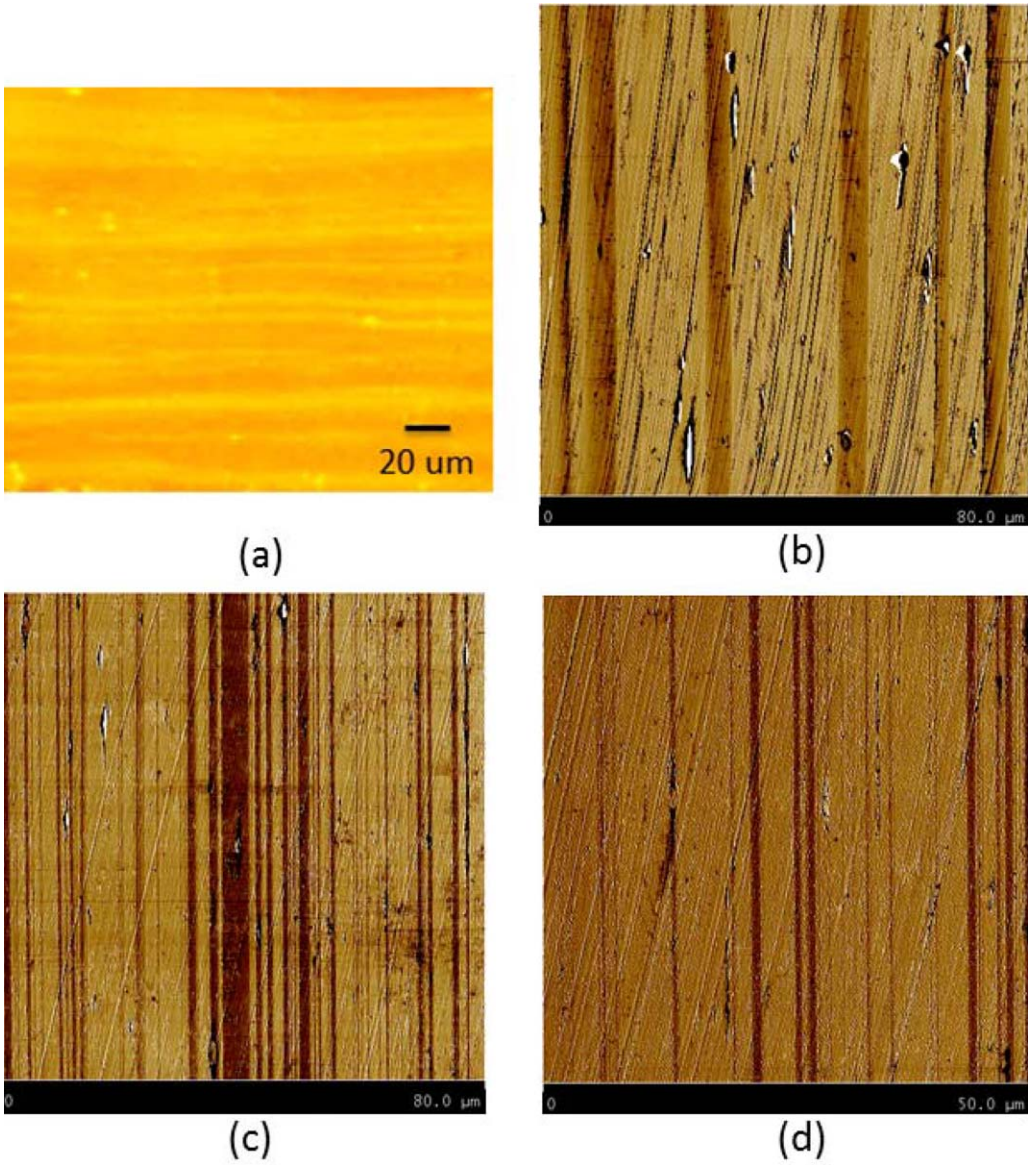

Figure 4. Morphologies of nominal 65-layer TPU B/TPU A films: (a) OM picture of film as extruded; AFM phase images of (b) extruded, (c) 75% stretched, and (d) 300% stretched films. [Color figure can be viewed in the online issue, which is available at wileyonlinelibrary.com.]

highly focused monochromatic CuKa ($\lambda = 0.1542$ nm) generated from a microfocus X-ray generator (Rigaku, MicroMax-002, Woodlands, TX) that was equipped with two laterally graded multilayer optics side-by-side. This collimated monochromatic X-ray beam was operated at 45 kV and 0.88 mA by using three pinholes, with the diameter of the beam around 700 mm. The images then were taken by using Fujifilm magnetic imaging plates and were processed by a Fujifilm FLA-7000 image plate reader. In order to obtain strong reflection patterns, extruded and stretched films were exposed for 8 and 16 h, respectively.

TPU films were embedded and fixed in epoxy that is cured at room temperature for 1 day. A Leica microsystmes EM FC6 ultramicrotome (Buffalo Grove, IL) was used to microtome the cross sections of TPU films at −70°C with direction perpendicular to extrusion. The layer uniformity of extruded and strectched 65-layer TPU films were charaterized by optical microscopy (OM) with an Olympus (Miami, FL) BH-2 optical microscope and a CCD camera. Mono-layer TPU films were examined with a Digital Laboratories Nanoscope IIIa AFM (Digital Instruments, Santa Barbara, CA) operating in tapping mode at room temperature. AFM phase and height images were analyzed *via* the NanoScope software to obtain modulus differences and morphology information.

The oxygen permeability measurements of TPU films were conducted by a MOCON OX-TRAN 2/20 (Minneapolis, MN) at 25°C, 0% relative humidity, and 1 atm pressure. Prior to testing, Mylar film (NIST certified) with known oxygen permeability was used to calibrate the Mocon machine. Then, both sides of the

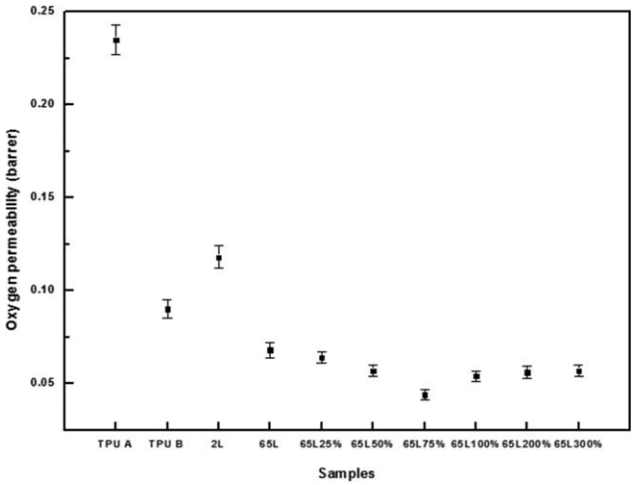

Figure 5. Oxygen permeability of extruded and stretched TPU films.

TPU films were masked by self-adhesive aluminum masks with a testing area of 5 cm^2 at the center. Nitrogen was used to remove the atmospheric oxygen inside the chamber for 12 hours.

The oxygen permeability $P(O_2)$ was calculated from the equation below:

$$P(O2)=J\frac{l}{\Delta P}$$

in which, J is the steady state flux minitored by Mocon machine, l is the total thickness of TPU film, and ΔP is the oxygen pressure difference across the film (1 atm). The unit of permeability used in this article is Barrers.

RESULTS AND DISCUSSION

Rheological Properties

The rheologically mismatched hard/soft TPU system with viscosity ratio over 10 and elasticity ratio of 100 at shear rate/frequency of 1 s^{-1} during co-extrusion [Figure 1 (a,b)], were successfully layered to 65-layer films with dimension of 7.5 cm (width) × 0.035 cm (thickness). Extensional rheological tests are also performed on these two TPUs. In Figure 1(c,d), TPU A shows strain-hardening behavior at all deformation rates, while TPU B mostly exhibits strain-softening except at the highest deformation rate of 10 s^{-1}. The reason for the high melt strength of TPU A is the long-range order caused by phase seperation between soft and hard segments. The strong intermolecular interaction leads to high extensional viscosity during stretching. On the other hand, TPU B, as an amorphous glassy TPU, consists of bulky polymer chains and yields to the deformation quickly, except at a very high deformation rate, where long-range, crystalline-like structures develop.[36]

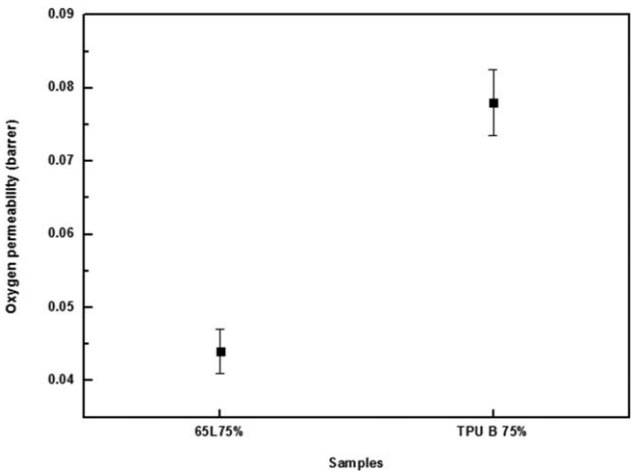

Figure 6. Oxygen permeability of 75% stretched TPU films.

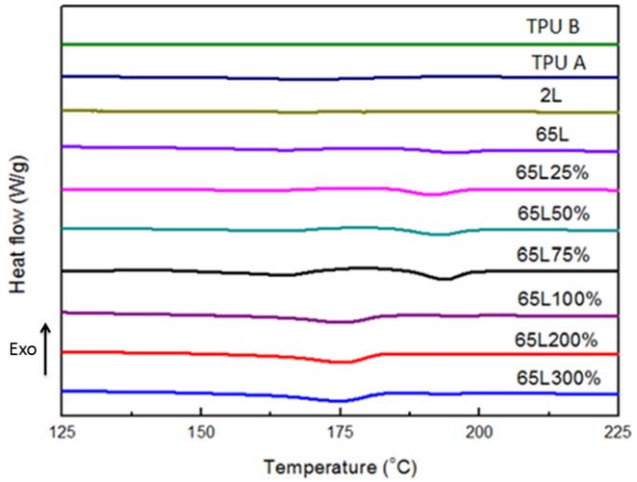

Figure 7. DSC results of extruded and stretched TPU films (heating rate-10°C/min^{-1}). [Color figure can be viewed in the online issue, which is available at wileyonlinelibrary.com.]

Morphology

The morphologies of mono-, bi-, and multilayer TPUs films are charaterized by optical microscopy and AFM. As shown in Figure 2, while TPU A shows long-range order in which bright areas represent the hard domaines and the black parts are the soft domaines, TPU B shows an amorphous structure. Because of the chemical compatibility of TPUs, interdiffusion between

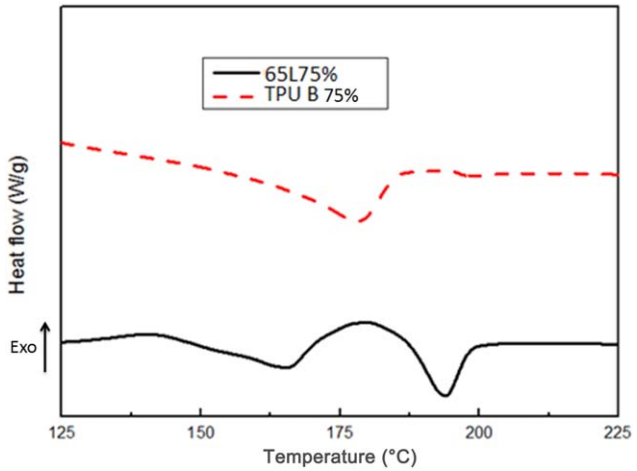

Figure 8. DSC results of 75% stretched TPU films (heating rate=10°C/min^{-1}). [Color figure can be viewed in the online issue, which is available at wileyonlinelibrary.com.]

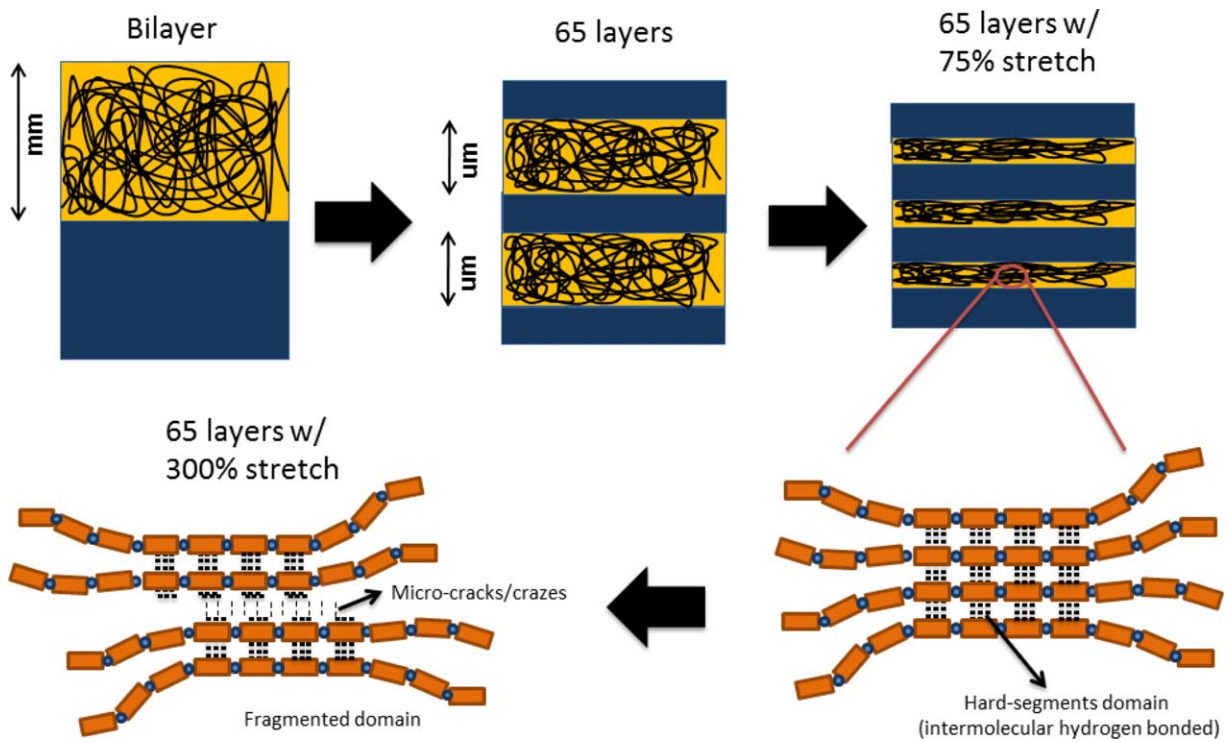

Figure 9. Schematic illustration for microconfinement effect on forming "hard-segment domain" in TPU B layer, and microscopic fracture at very high deformation, in which the yellow layer is TPU B and the dark blue layer is TPU A, orange boxes are the di-isocyanate and light blue spots are chain extenders. [Color figure can be viewed in the online issue, which is available at wileyonlinelibrary.com.]

TPU B and TPU A layer is expected and the cross-section of the bi-layer TPU film shown in Figure 3, in which an interphase with 2-μm width is observed.[37]

AFM phase images of nominal 65-layer TPU films (in Figure 4) reveal that good multilayered structures are achieved for both extruded and stretched films. In Figure 4(b), for example, there are 13 layers. The reader is looking at the actual layers because all the samples were cut at an angle with the surface of the glass knife, so the microtome marks are inclined in the AFM pictures. The composition or layer thickness ratio is not 50/50 as expected because: (a) despite the use of a balanced multiplier die and external lubricants there is still some residual encapsulation of the high-viscosity TPU B by the low-viscosity TPU A; (b) The 9-layer feedblock used in this study yields different flow rates in the TPU B and the TPU A channels, because the total flow rates are the same and the TPU B flows through five channels, while the TPU A flows through four. However, taking into consideration that the viscoelastic ratio of two TPUs is around 100, the multilayered structure created is a notable success.

Gas Barrier Properties

Gas (oxygen) permeabilities of mono and multilayer TPU films are shown in Figures 5 and 6. As expected, the rigid TPU B has superior barrier properties than TPU A because of the higher percentage of hard segments. While the bilayer film exhibits a permeability between the two TPUs, the nominal 65-layer film shows much lower permeability than TPU B. The 65-layer TPU film has a nominal individual layer thickness of approximately 6 μm and undergoes simultaneous squeezing and spreading in the multiplier dies, leading to microconfinement and, hence, lower O_2 permeability. On a lesser scale, it is the same effect as after stretching. The multilayer films were further uniaxially stretched to different strains at 100°C. The stretched multilayer films show a decrease in permeability as the deformation increases up to 75% and an increase afterwards, up to the maximum stretch of 300%. Thus, the best gas barrier properties of 0.044 barrer were found for the 65-layer film with 75% stretch at this temperature. This represents an almost three-fold improvement relatively to the bilayer film, which has permeability of 0.12 barrer, and a five-fold improvement relatively to TPU A, which has a permeability of 0.235 barrer. Interestingly these variations of gas permeability with stretch are not observed if the monolayer TPU B film is uniaxially stretched. The explanation for this phenonmena will be discussed in next paragraphs.

Thermal Properties

The thermal properties of TPU films measured by DSC can be used to shed light on the observed tendency in oxygen permeability. In Figures 7 and 8, there are three pronounced endotherm peaks at 165°C, 175°C, and 195°C, representing dissociation of long-range order in TPU A, fragmented hard-segment domains (see below), and main hard-segment domains in TPU B, respectively.[5–7,38,39] While both monolayer and bilayer TPU films show almost no endothermal peak around 195°C, co-extruded and stretched (up to 75%) multilayer TPU films exhibit large peaks at this temperature. Further stretching from 100% to 300% on the multilayer films

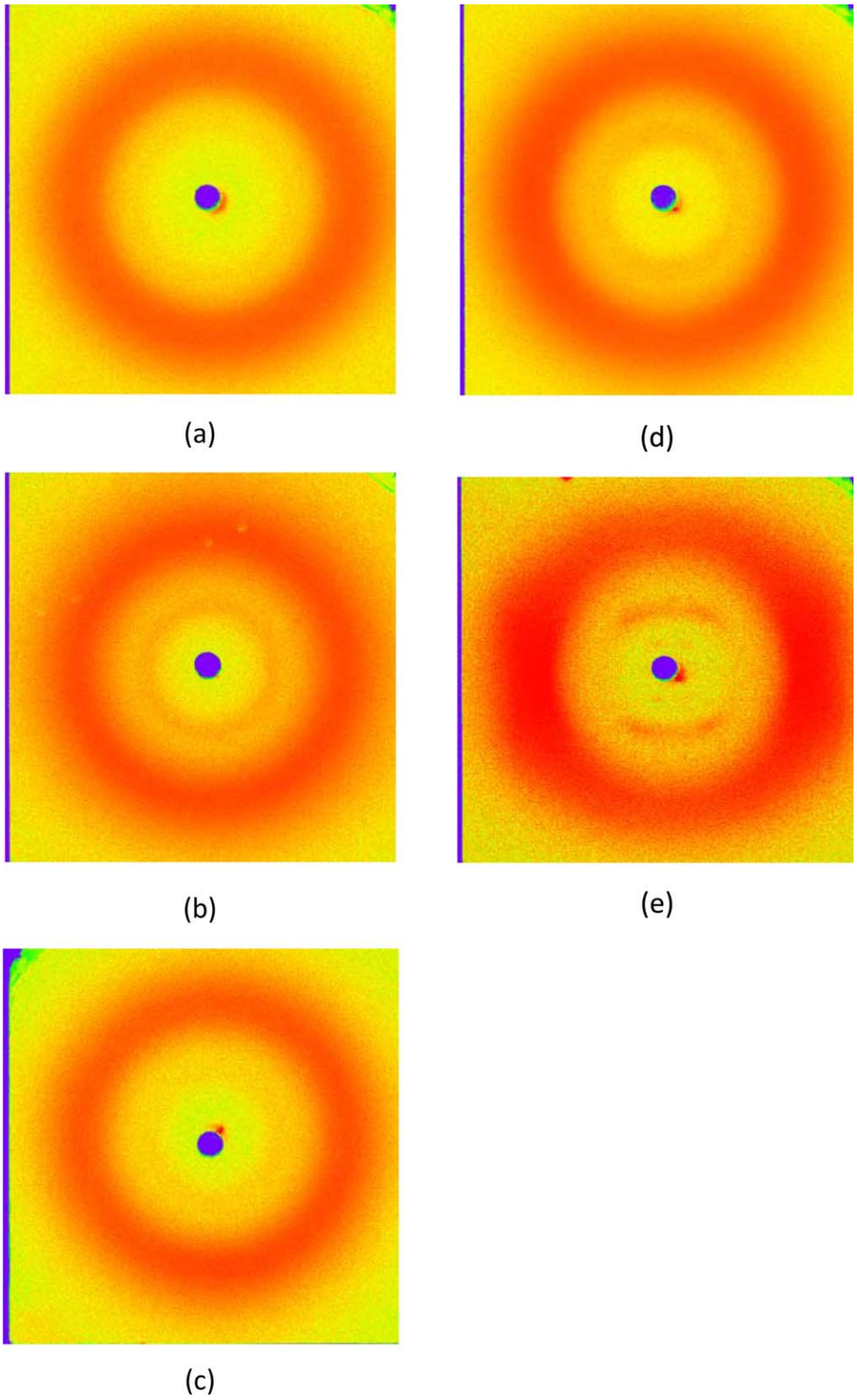

Figure 10. Normal direction 2-D WAXS patterns for various TPU films: (a) TPU A, (b) TPU B, (c) 65-layer, (d) 65-layer with 75% stretch, and (e) nominal 65-layer with 300% stretch. [Color figure can be viewed in the online issue, which is available at wileyonlinelibrary.com.]

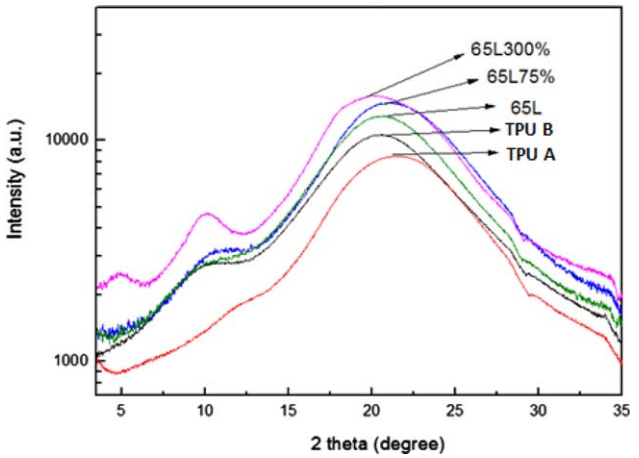

Figure 11. 1-D WAXS profiles of various TPU films. [Color figure can be viewed in the online issue, which is available at wileyonlinelibrary.com.]

makes the endothermal peak shift from 195°C to 175°C. When 75% stretched monolayer TPU B film and multilayer film are compared, the former only shows a tiny bump around 195°C.

Based on the permeability and thermal results of TPU films, the mechanism of enhanced barrier properties is proposed as shown in Figure 9. When mono or bilayer TPU film are extruded, the TPU chains, especially in TPU B, with isotropic and bulky structure because of the thick individual layer thickness are not able to form impermeable "hard-segments domains" connected by intermolecular hydrogen bondings between "–NH" and "C=O" groups along the backbone.[38,39] Once the TPUs are layered into multilayer structure with individual layer thickness around 6 μm, under microconfinement the polymer chains are oriented through the simultaneous squeezing and spreading process that occurs in multiplier dies, which begins constructing "hard-segment domains". The multilayer films are then stretched to 75% to further orient the polymer chains building up even more organized "hard-segments domains", which reduces the permeability by making a tortuous path for oxygen molecules to pass through the films. On the other hand, mono-

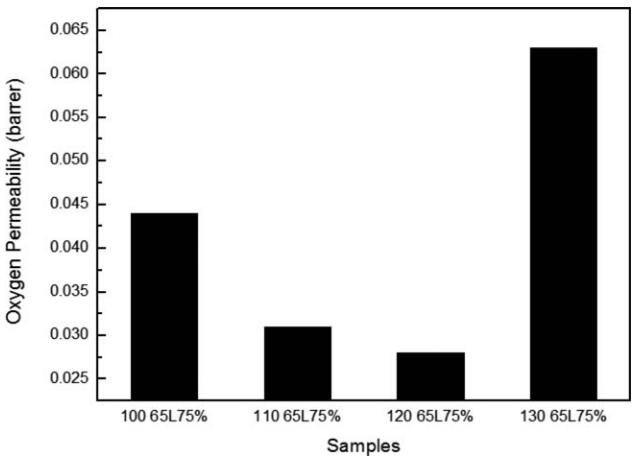

Figure 12. Oxygen permeability of 75% stretched nominal 65-layer film as function of temperatures.

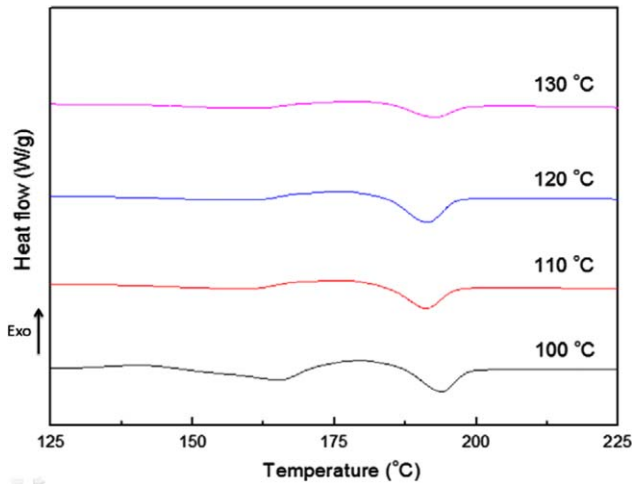

Figure 13. DSC results of nominal 65-layer film with 75% stretching at different temperatures. [Color figure can be viewed in the online issue, which is available at wileyonlinelibrary.com.]

layer TPU B with the same 75% stretching is not able to form such "hard-segments domains", and reduce the gas permeability, because of the lack of oriented polymer chains under microconfinement. Stretching the multilayer TPU films from 100% to 300% creates microcracks in the "hard-segment domains". Instead of producing more densly packed structures, microcrazes start to appear, causing the gas permeabilities increase.[38]

Wide Angle X-ray Scattering

In order to confirm the structural model, WAXS measurements in both the normal and transverse directions were performed on extruded and stretched TPU films. 2-D WAXS patterns of monolayer TPU B, TPU A and multilayer films are provided in Figure 10. In this, all TPU films show a broad amorphous halo and a sharp diffraction ring. In TPU A where the long-range order is observed by AFM and DSC, the sharp ring represents the "hard-segments domains" that have a *d*-spacing of 7.38 Å, which is in agreement with the results reported by Yunxin *et al.*[7] As mentioned before, the long length and high ratio of soft segments facilitate microphase seperation and the formation of ordered "hard-segments domains". Compared to TPU A, the sharp ring in TPU B appears at a place closer to the center meaning a slightly larger *d*-spacing (=8.84 Å) between the hard-segments sheets because it has no soft segments.

While the extruded multilayer film [Figure 10(c)] exhibit the overlapped diffraction rings consisting of those in TPU B and TPU A, the multilayer film with 75% stretch [Figure 10(d)]

Table I. Comparison of Integrated Endothermic Peak of "Hard-Segments Domains" in Nominal 65-Layer Film with 75% Stretching at Different Temperatures

Temperature	Integrated peak (J/g)
100°C	9.98
110°C	12.20
120°C	12.41
130°C	5.9

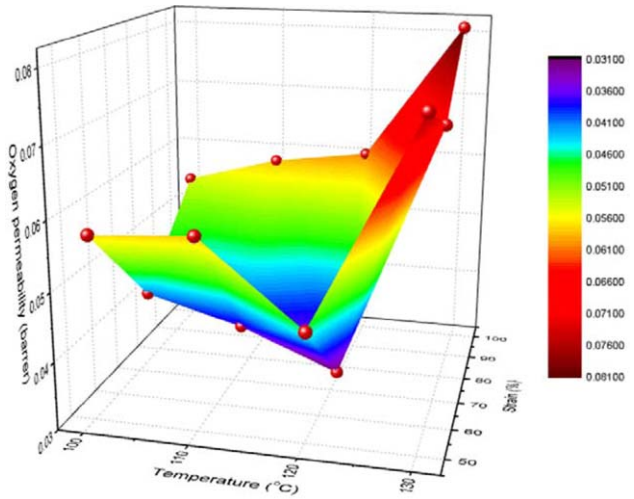

Figure 14. 3-D profile on oxygen permeability of nominal 65-layer film depending on stretching ratio and temperatures. [Color figure can be viewed in the online issue, which is available at wileyonlinelibrary.com.]

shows broad reflection arcs at the meridian in the center of the pattern presenting the oriented polymer chains. This trend can be more clearly seen in 1-D WAXS profile as shown in Figure 11, in which the multilayer film shows a broad peak between the ones of two controlled TPU films at 2θ of 10° and 12°. This peak becomes broader and more pronounced when the multilayer film is 75% stretched. The reason is attributed to the fact that the stretching under microconfinement facilitates further polymer chain orientation forming more and denser "hard-segment domains". When the multilayer film is stretched beyond 75% (i.e. to 300%), even though the arcs in the WAXS pattern become sharper and sharper, a new pair of arcs at 2θ of 4.8° appear because of the fragmented "hard-segment domains" [Figure 10(e)].

Gas Barrier Properties Dependence on Stretching Temperature

The multilayer TPU films were stretched at different temperatures to examine the gas barrier properties dependence on stretching temperature. As can be seen in Figure 12, with the same amount of stretching, i.e. 75%, the permeability decreases as the temperature increases up to 120°C. It is at this stretching temperature that the lowest permeability of 0.028 barrer is achieved, which is an eight-fold improvement relative to TPU A, four-fold relative to the bilayer film, and three-fold relative to TPU B. However, the permeability increases when the stretching temperature is elevated to 130°C. As mentioned before, the enhancement of gas barrier properties is because of the impermeable "hard-segments domains" that are formed by intermolecular hydrogen bonds. When the temperature is elevated from 100°C to 120°C, the mobility of TPU chains increases, and the possibility to form "hard-segments domains" becomes higher. This can be proven by DSC as shown in Figure 13 and Table I; the integrated endothermic peak of "hard-segments domains" increases from 9.98 to 12.41 J/g between 100°C and 120°C. On the other hand, at 130°C the "hard-segments domains" are destroyed because of the high energy that deconstructs the intermolecular hydrogen bonds, which is in agreement with the findings of Coleman *et al.*[39] Finally, Figure 14 shows the overall dependency of permeability of multilayer TPU films on temperature and stretching ratio, and the set of conditions that lead to the lowest permeability is 75% stretching at 120°C.

Mechanical Properties

The effect of microconfinement on mechanical properties is also pronounced. The stress–strain curve and the tensile properties for mono-, bi-, and multilayer TPU films at room temperature are summarized in Figure 15 and Table II. As expected, the rigid TPU B has a high yield stress and a low elongation at break of 95.69%, while the TPU A shows a ductile mechanical behavior. The bilayer, like the gas barrier properties, posseses mechanical properties in-between those of the two components. However, the multilayer film not only shows a high yield stress of 29.17 MPa, but also a high elongation at break that is close to 195%, a strong and ductile behavior with toughness about 76.07 MPa, and the highest fracture stress at 60.49 MPa. These

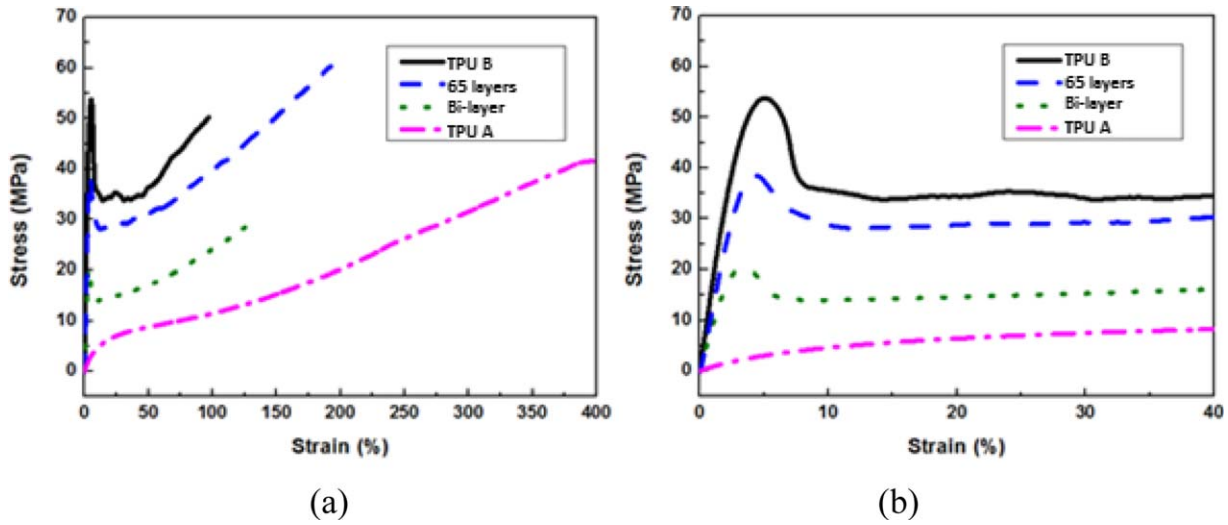

Figure 15. Stress–strain curves for various TPU films: (a) full scale, and (b) initial area zoomed in. [Color figure can be viewed in the online issue, which is available at wileyonlinelibrary.com.]

Table II. Mechanical Properties of Extruded TPU Films

	Elastic modulus (MPa)	Elongation at break (%)	Fracture stress (MPa)	Yield stress (MPa)	Toughness (MJ/m^3)
TPU B	1867.24 ± 98.46	95.69 ± 9.81	46.63 ± 3.81	35.02 ± 3.15	32.02 ± 6.09
TPU A	109.61 ± 3.19	397.86 ± 6.25	41.64 ± 2.23	2.18 ± 0.12	89.61 ± 5.04
Bi-layer	1032.75 ± 100.34	127.40 ± 15.38	34.26 ± 6.86	20.51 ± 2.13	36.65 ± 11.40
65 layers	1265.13 ± 2.38	193.25 ± 1.64	60.49 ± 0.19	29.17 ± 0.71	76.07 ± 2.36

improvements are because of the fact that the stress relief based on the interaction of the microcracks in TPU B with TPU A layers is able to alleviate crazing.[27,40]

CONCLUSIONS

Extruded and stretched nominal 65-layer rigid/soft TPU films were successfully produced through a novel layer-multiplying co-extrusion and uniaxial stretching and the dependence of gas permeability on deformation and temperature was studied. Uniaxial stretching under microconfinement has a significant effect on gas barrier properties of TPUs, with up to an eight-fold improvement of 75% stretched multilayer film when compared to the component polymers. Such a reduction in gas permeability is because of oriented "hard-segment domains" in the TPU B layers resulting from intermolecular hydrogen bonds connected between "-NH" and "C=O" groups along the TPU A backbones. This makes the gas-diffusion pathway more tortuous. Multilayer TPU films with stretching beyond 75%, instead of further improving the gas barrier properties, increase the permeability because the "hard-segment domains" start to break up under these circumstances. Finally, the microconfinement also shows effect on mechanical properties, with 100% improvement on elongation at break being found from TPU B monolayer to 65-layer TPU film, because the interaction of the microcraks in TPU B with TPU A layers is able to alleviate crazing.

ACKNOWLEDGMENTS

The authors wish to acknowledge Lubrizol Advanced Materials, Inc. and CLiPS – Center for Layered Polymeric Systems, an NSF Science and Technology Center, grant #0423914, for the funding provided.

REFERENCES

1. Furukawa, M.; Mitsui, Y.; Fukumaru, T.; Kojio, K. *Polymer* **2005**, *46*, 10817.
2. Kojio, K.; Kugumiya, S.; Uchiba, Y.; Nishino, Y.; Furukawa, M. *Polym. J.* **2009**, *41*, 118.
3. Tang, D.; Macosko, C. W.; Hillmyer, M. A. *Polym. Chem.* **2014**, *5*, 3231.
4. Chattopadhyay, D. K.; Raju, K. V. S. N. *Prog. Polym. Sci.* **2007**, *32*, 352.
5. Chen, T. K.; Shieh, T. S.; Chui, J. Y. *Macromolecules* **1998**, *31*, 1312.
6. Bajsic, E. G.; Rek, V.; Sendijarevic, A.; Sendijarevic, V.; Frisch, K. C. *J. Elastom. Plast.* **2000**, *32*, 162.
7. Wang, Y.; Gupta, M.; Schiraldi, D. A. *J. Polym. Sci. Part B Polym. Phys.* **2012**, *50*, 681.
8. Gisselfalt, K.; Helgee, B. *Macromol. Mater. Eng.* **2003**, *288*, 265.
9. Mishra, A.; Maiti, P. *J. Appl. Polym. Sci.* **2011**, *120*, 3546.
10. Prisacariu, C. Polyurethane Elastomers: From Morphology to Mechanical Aspects; Springer: New York, **2011**.
11. Tseng, J.-K.; Tang, S.; Zhou, Z.; Mackey, M.; Carr, J. M.; Mu, R.; Flandin, L.; Schuele, D. E.; Baer, E.; Zhu, L. *Polymer* **2014**, *55*, 8.
12. Lin, Y.; Hiltner, A.; Baer, E. *Polymer* **2010**, *51*, 5807.
13. Zhang, G.; Lee, P. C.; Jenkins, S.; Dooley, J.; Baer, E. *Polymer* **2014**, *55*, 663.
14. Cheng, W.; Gomopoulos, N.; Fytas, G.; Gorishnyy, T.; Walish, J.; Thomas, E. L.; Hiltner, A.; Baer, E. *Nano Lett.* **2008**, *8*, 1423.
15. Ji, S; Yin, K; Mackey, M; Brister, A; Ponting, M; Baer, E. *Opt. Eng.* **2013**, *52*, 112105.
16. Lai, C.-Y.; Ponting, M. T.; Baer, E. *Polymer* **2012**, *53*, 1393.
17. Singer, K. D.; Kazmierczak, T.; Lott, J.; Song, H.; Wu, Y.; Andrews, J.; Baer, E.; Hiltner, A.; Weder, C. *Opt. Express.* **2008**, *16*, 10358.
18. Ryan, C.; Christenson, C. W.; Valle, B.; Saini, A.; Lott, J.; Johnson, J.; Schiraldi, D.; Weder, C.; Baer, E.; Singer, K. D.; Shan, J. *Adv. Mater.* **2012**, *24*, 5222.
19. Lott, J.; Ryan, C.; Valle, B.; Johnson, J. R.; Schiraldi, D. A.; Shan, J.; Singer, K. D.; Weder, C. *Adv. Mater.* **2011**, *23*, 2425.
20. Wang, H.; Keum, J. K.; Hiltner, A.; Baer, E. *Macromolecules* **2009**, *42*, 7055.
21. Zhang, G.; Baer, E.; Hiltner, A. *Polymer* **2013**, *54*, 4298.
22. Langhe, D. S.; Hiltner, A.; Baer, E. *Polymer* **2011**, *52*, 5879.
23. Wang, H.; Keum, J. K.; Hiltner, A.; Baer, E.; Freeman, B.; Rozanski, A.; Galeski, A. *Science* **2009**, *323*, 757.
24. Carr, J. M.; Mackey, M.; Flandin, L.; Schuele, D.; Zhu, L.; Baer, E. *J. Polym. Sci. Part B Polym. Phys.* **2013**, *51*, 882.
25. Burt, T. M.; Keum, J.; Hiltner, A.; Baer, E.; Korley, L. T. J. *ACS Appl. Mater. Interfaces* **2011**, *3*, 4804.
26. Sheng, D.; Tan, J.; Liu, X.; Wang, P.; Yang, Y. J. *Mater. Sci.* **2011**, *46*, 6508.
27. Lai, C. -Y.; Hiltner, A.; Baer, E.; Korley, L. T. J. *ACS Appl. Mater. Interfaces* **2012**, *4*, 2218.
28. Carr, J. M.; Langhe, D. S.; Ponting, M. T.; Hiltner, A.; Baer, E. *J. Mater. Res.* **2012**, *27*, 1326.

29. Carr, J. M.; Mackey, M.; Flandin, L.; Hiltner, A.; Baer, E. *Polymer* **2013**, *54*, 1679.

30. Koerner, H.; Kelley, J. J.; Vaia, R. A. *Macromolecules* **2008**, *41*, 4709.

31. Shibayama, M.; Inoue, M.; Yamamoto, T.; Nomura, S. *Polymer* **1990**, *31*, 749.

32. Huang, R.; Patz, J.; Silva, J.; Maia, J. M.; Huntington, B. A.; Bonnecaze, R. T.; Cox, M. ANTEC **2014** Proceedings. April 27–30, Las Vegas, to appear.

33. Huang, R.; Patz, J.; Silva, J.; Andrade, R.; Harris, P.; Yin, K.; Huntington, B.; Bonnecaze, R.; Cox, M.; Maia, J. M. *Int. Polym. Proc.,* to appear.

34. Barroso, V.; Covas, J. A.; Maia, J. M. *Rheol. Acta* **2002**, *41*, 154.

35. Harris, P. J.; Patz, J.; Huntington, B. A.; Bonnecaze, R. T.; Meltzer, D.; Maia, J. *Polym. Eng. Sci.* **2014**, *54*, 636.

36. Silva, J.; Andrade, R.; Huang, R.; Liu, J.; Meltzer, D.; Cox, M.; Maia, J. M. *J. NonNewtonian Fluid Mech.* **2014**, submitted.

37. Silva, J.; Maia, J. M.; Huang, R.; Meltzer, D.; Cox, M.; Andrade, R. *Rheol. Acta* **2012**, *51*, 947.

38. Sakurai, S.; Yoshida, H.; Hashimoto, F.; Shibaya, M.; Ishihara, H.; Yoshihara, N.; Nishitsuji, S.; Takenaka, M. *Polymer* **2009**, *50*, 1566.

39. Coleman, M. M.; Lee, K. H.; Skrovanek, D. J.; Painter, P. C. *Macromolecules* **1986**, *19*, 2149.

40. Ponting, M.; Burt, T. M.; Korley, L. T. J.; Andrews, J.; Hiltner, A.; Baer, E. *Ind. Eng. Chem. Res.* **2010**, *49*, 12111.